GEOPHYSICAL RESEARCH LETTERS, VOL. 23, NO. 21, PAGES 2967-2970, OCTOBER 15, 1996

Baroclinic wave variations observed in MLS upper tropospheric water vapor

Elizabeth M. Stone and William J. Randel
National Center for Atmospheric Research, Boulder, Colorado

John L. Stanford
Department of Physics and Astronomy, Iowa State University, Ames

William G. Read and Joe W. Waters
Jet Propulsion Laboratory, California Institute of Technology, Pasadena

Abstract. Upper tropospheric water vapor measurements from the UARS Microwave Limb Sounder are used to investigate the structure and evolution of eastward traveling medium-scale wave features in Southern Hemisphere summertime. The extratropical Southern Hemisphere summer circulation pattern is frequently dominated by medium scale waves which exhibit life cycles of baroclinic growth and barotropic decay. The water vapor field during such life cycles is examined here and found to be well correlated with meteorological fields derived from European Centre for Medium Range Weather Forecasts global analyses. From mid January to mid February 1992 several episodes of growth and decay in the amplitude of eastward traveling waves are found in the water vapor and meteorological data at levels of the upper troposphere, with zonal waves four, five and six being predominant modes. The water vapor data are compared with derived potential vorticity (PV) fields, with strong anticorrelation observed in middle and high latitudes. The results are consistent with model paradigms for the structure and evolution of baroclinic disturbances, coupled with the known characteristics of high PV and low water vapor mixing ratios in lower stratospheric air parcels and the reverse for upper tropospheric air.

Introduction

The extratropical Southern Hemisphere (SH) summer circulation pattern is frequently dominated by medium scale waves (zonal wavenumbers 4-7), which propagate eastward with periods near 10 days [*Salby*, 1982; *Hamilton*, 1983; *Randel and Stanford*, 1985]. The medium scale waves often exhibit well defined life cycles of baroclinic growth and barotropic decay, and appear very similar to the idealized baroclinic waves studied by *Simmons and Hoskins* [1978], *Barnes and Young* [1992], and *Thorncroft et al.* [1993]. Northern Hemisphere baroclinic waves are commonly longitudinally localized along stormtrack regions [e. g., *Blackmon et al.*, 1984], whereas SH features often have wave maxima distributed more symmetrically around a latitude circle. These systems provide a dominant means of heat and momentum transport in the troposphere.

Since baroclinic waves are fundamental to tropospheric dynamics, they can be expected to impact atmospheric constituent distributions. *Schoeberl and Krueger* [1983] observed medium scale wave disturbances (zonal wave 5) in SH measurements of total column ozone from the Total Ozone Mapping Spectrometer (TOMS). *Mote et al.* [1991] find baroclinic wave signatures in TOMS ozone data along Northern Hemisphere oceanic stormtrack regions. Signatures of baroclinic waves have been studied

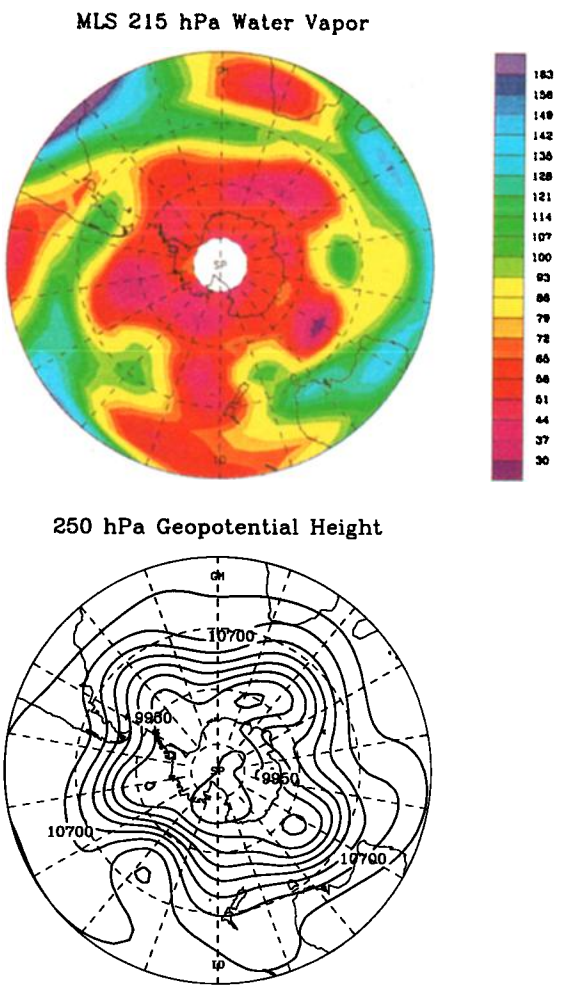

Figure 1. Polar plots of the SH for 20 January 1990. (a) MLS water vapor field (ppmv) at 215 hPa and (b) ECMWF 250 hPa geopotential height (m). Lines of constant latitude and longitude are drawn every 20 degrees. Meridional coverage is from 20°S to the pole. Geopotential height contours are incremented by 150 m.

Paper number 96GL02576.
0094-8534/96/96GL-02576$05.00

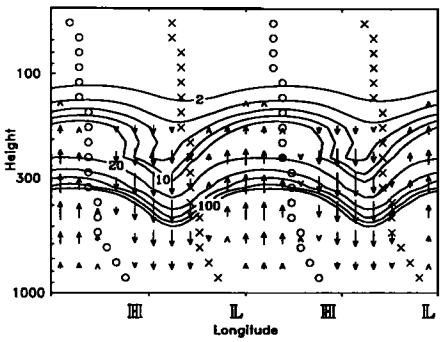

Figure 2. Schematic illustration of a developing baroclinic wave on a longitude-height cross section derived from an idealized life cycle simulation. Vectors represent vertical velocity; O and X represent the ridge and trough axis. Contours (2, 4,...10, 20,...100) are of water vapor mixing ratio in 10^{-6} kg/kg.

previously in tropospheric water vapor distributions derived from satellite observations of radiances in the 6-7 μm water vapor absorption bands [e. g., *Rodgers et al.*, 1976; *Appenzeller et al.*, 1996]. Measurements of this type have a broad vertical resolution and are sensitive to water vapor in approximately the upper third of the troposphere under clear sky conditions.

Elson et al. [1996] have examined space-time variability of upper tropospheric water vapor from the Microwave Limb Sounder (MLS) on the Upper Atmospheric Research Satellite (UARS) and have noted eastward traveling medium-scale waves during the SH summer. Our work extends that study by examining in more detail the medium scale waves during one month, including their association with meteorological fields derived from operational analyses.

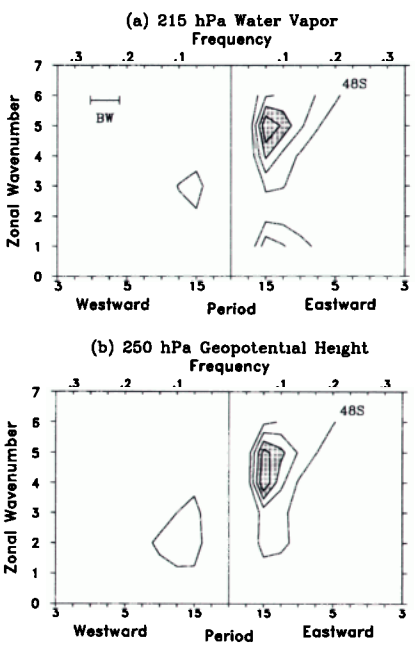

Figure 3. Zonal wavenumber versus frequency power spectra at 48°S for (a) MLS water vapor and (b) ECMWF geopotential height. Contours are drawn at 20%, 40%, ... 100% of the maximum value. Regions of 60% and larger are shaded. Labels along the abscissa are periods in days and frequencies in day^{-1}. The spectral band width (BW) is shown.

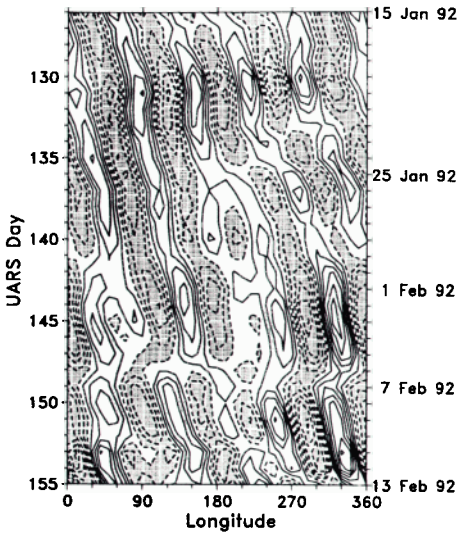

Figure 4. Time versus longitude diagram of zonal waves 4-6 MLS water vapor at 44°S and 215 hPa. Solid (dashed) contours in ppmv begin at 3.0 (-3.0) and increment (decrement) by 6.0. Regions with negative perturbation mixing ratio are shaded.

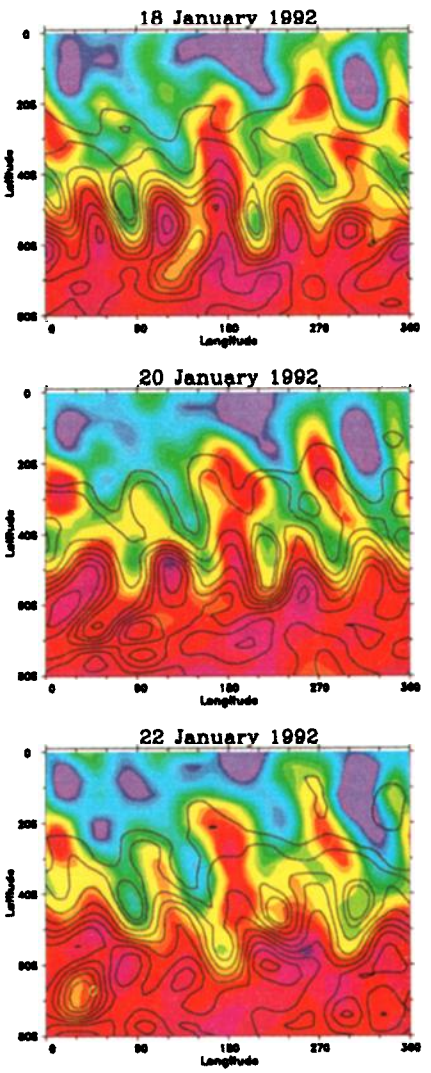

Figure 5. Latitude-longitude plots of upper tropospheric water vapor and PV for January 18, 20, 22, 1992. Color contours (scale shown in Fig. 2) show the MLS water vapor field at 215 hPa. Overlaid contours denote the negative PV field (0.5, 1, 2, ...PVU, 1 PVU=10^{-6} m^2 K s^{-1} kg^{-1}).

Data

The Microwave Limb Sounder [*Barath et al.*, 1993] observes emissions at the limb of the atmosphere simultaneously in spectral bands at 63, 183, and 205 GHz. When the 205 GHz spectral band is scanned down through the troposphere, the dominant contribution to its measured signal is thermal emission from water vapor. The retrieval process for the preliminary upper tropospheric water vapor data analyzed here is reported by *Read et al.* [1995]. The vertical resolution of the data is limited by the instrument's 3 km field of view. Retrievals are made on 4 vertical levels in the upper troposphere (464 hPa, 315 hPa, 215 hPa, and 146 hPa). The best sensitivity to water vapor occurs where the abundances are ~100-300 ppmv which corresponds to altitudes near 12 km at low latitudes and 7 km at high latitudes. Although the data have yet to be systematically validated, *Read et al.* [1995] find reasonable agreement among comparisons of the MLS water vapor with modeled and assimilated data and demonstrate that the water vapor fields are able to track synoptic scale variability. Reasonable agreement is found in comparisons of the MLS upper tropospheric water vapor measurements with in situ aircraft measurements [*Newell et al.*, 1995].

The data analyzed here have been synoptically mapped using a Kalman filter technique which gives once daily values for the zonal mean and the coefficients for zonal waves 1-6 with meridional resolution of 4°. This study focuses on the 215 hPa vertical level for the month of 15 January-13 February 1992. During this time the MLS instrument covered the latitude range of 80°S-34°N. The meteorological fields used in this study are taken from the archive of European Centre for Medium Range Weather Forecasts (ECMWF) global analyses described by *Trenberth* [1992]. The data have been truncated to zonal waves 0-6 to match the resolution of the MLS data.

Observed Medium Scale Wave Features

Figure 1a shows a synoptic map of the MLS upper tropospheric water vapor data at 215 hPa on 20 January 1992. A zonal wavenumber 5 pattern clearly dominates the midlatitudes. The maximum amplitude of this wave exists at 48°S where the perturbation is 38% of the zonal mean value for this latitude. A marked medium scale wave structure, with any of zonal waves 4, 5 or 6 being predominant, is discernible for many of the days considered in this study. The ECMWF analysis of 250 hPa geopotential height for this day, is shown in Figure 1b. There is a strong correlation between the water vapor and geopotential data over midlatitudes, with troughs in the height field aligned with regions of low water vapor mixing ratio and positive perturbations in water vapor corresponding to the height ridge lines.

The schematic in Figure 2 depicts the synoptic scale structure of a developing baroclinic wave produced from an idealized nonlinear baroclinic wave life cycle simulation (a zonal wavenumber 6 life cycle simulated using the NCAR CCM2, similar to the model results of *Simmons and Hoskins* [1978]; details to be reported elsewhere). This idealized simulation demonstrates how water vapor fields in the upper troposphere are related to dynamical structure in a developing baroclinic wave. The trough and ridge axis, which tilt westward with increasing height, the vertical velocity, and the water vapor field are displayed for two zonal wavelengths. Air descending west of the surface low pressure originates from higher altitudes and is very dry. In front (east) of the surface low, warm and moist air rises. In the region of the upper troposphere and lower stratosphere, where values of water vapor mixing ratio drop off rapidly with increasing height, there is a strong correlation between the water vapor and geopotential height fields.

In order to quantify the spectral content of traveling waves in these data, we calculate space-time power spectra according to the technique of *Hayashi* [1971]. Figure 3 shows zonal wavenumber-frequency sections at 48°S of eastward and westward spectral power for the water vapor and geopotential height data sets. The two fields have similar signals with maxima occurring in eastward propagating zonal waves 4-5 with periods of 10-15 days. Calculations of cross spectra between the two fields (not shown) reveal significant coherence and near zero phase difference for eastward propagating, medium scale wave features with periods longer than 5 days.

Figure 4 shows a time versus longitude diagram for the water vapor data at 44°S, constructed from zonal waves 4-6. This illustrates several episodes of wave growth and decay and regular eastward phase movement throughout the record. Note that no time filtering was used to construct Figure 4. Nearly identical patterns are observed in the geopotential height data (not shown). The first event, occurring over January 17-22, is dominated by zonal wave 5. Two growth and decay episodes are also seen in February encompassing zonal waves 4, 5 and 6.

Comparison with Potential Vorticity

Baroclinic waves are often characterized by potential vorticity (PV) anomalies in the upper troposphere [*Hoskins et al.*, 1985; *Thorncroft et al.*, 1993; *Hartmann*, 1995]. Because PV acts as a tracer of fluid motions on advective time scales, it is of interest to quantify the relationship between PV and the water vapor data here.

Figure 5 shows a time sequence (over January 18-22) of the water vapor field with contours of the absolute value of PV on the 250 hPa surface overlaid. The PV=2 PVU approximately denotes the boundary between the troposphere and stratosphere. A prominent zonal wave 5 is seen in the midlatitude PV and water vapor fields on these days. Meridional gradients of the two tracers are aligned and out of phase. Large values of PV, denoting stratospheric air, correspond to low water vapor mixing ratios, and conversely water vapor values indicative of moist tropospheric air coincide with regions of low PV. This overall agreement between the midlatitude wave structure of the two fields is typical for the days comprising this study.

To quantify the PV-water vapor mixing ratio coherence, Figure 6 shows a scatter diagram of the two fields sampled over the 40°S-60°S latitudinal range and the 30 days included in this study.

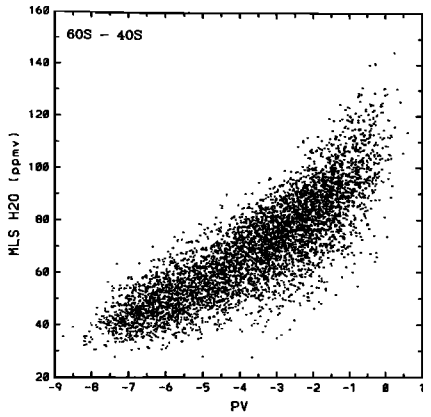

Figure 6. Scatter diagram comparing the upper tropospheric MLS water vapor mixing ratio (ppmv) at 215 hPa versus the calculated PV field (PVU) at 250 hPa over the latitudinal range of 40°S-60°S, sampled over the 30 days in the study.

As anticipated, an approximate anticorrelation of the two fields is observed. However, there is significant scatter in the figure which shows that although the water vapor and PV fields are related, it is not a compact correspondence. We find similar scatter in PV-water vapor correlations derived from the idealized model results discussed above in relation to Figure 2, suggesting the scatter in Figure 6 is not due solely to instrumental or sampling effects.

The sequence of days in Figure 5 shows the medium scale waves in the water vapor and PV extending over a wide meridional range (60°S-20°S). The observed spatial structure suggests that there may be some relationship between variations in the subtropical regions and middle latitudes. Regions of detached dry air, with mixing ratios typical of the middle and high latitudes or of higher altitudes, are found in the subtropical region. The waves equatorward of 30°S are quasi-stationary in contrast to the eastward traveling perturbations in the middle latitudes.

Summary

A case study analysis of UARS MLS upper tropospheric water vapor measurements in the SH summertime reveals large amplitude medium scale wave features. Maximum power in the midlatitudes is found in eastward traveling zonal waves 4-5 with periods of 10-15 days and these features are shown here to be associated with traveling baroclinic waves. The features compare well with similar structure found in ECMWF geopotential height and PV fields in agreement with the upper level development of a baroclinic wave. Recognizing distinct synoptic scale features in the relatively new MLS tropospheric water vapor data set attests to its usefulness for upper tropospheric studies.

Acknowledgments. This work was supported under NASA grants W-16215, W-18181, and NAG 5-2787. The research performed at the California Institute of Technology Jet Propulsion Laboratory was under contract with NASA and sponsored through its UARS project. The National Center for Atmospheric Research is sponsored by the National Science Foundation.

References

Appenzeller, C., H. C. Davies, and W. A. Norton, Fragmentation of stratospheric intrusions, *J. Geophys. Res.*, *101*, 1435-1456, 1996.

Barath, F. T., et al., The upper atmosphere research satellite microwave limb sounder instrument, *J. Geophys. Res.*, *98*, 10,751-10,762, 1993.

Barnes, J. R., and R. E. Young, Nonlinear baroclinic instability on a sphere: Multiple life cycles with surface drag and thermal damping, *J. Atmos. Sci.*, *49*, 861-878, 1992.

Blackmon, M. L., Y.-H. Lee, and J. M. Wallace, Horizontal structure of 500 mb height fluctuations with long, intermediate and short time scales, *J. Atmos. Sci.*, *41*, 961-979, 1984.

Elson, L. S., W. G. Read, J. W. Waters, P. W. Mote, J. S. Kinnersley and R. S. Harwood, Space-time variations in water vapor as observed by the UARS Microwave Limb Sounder, *J. Geophys. Res.*, *101*, 9001-9016, 1996.

Hamilton, K., Aspects of wave behavior in the mid and upper troposphere of the Southern Hemisphere, *Atmos. Ocean*, *21*, 40-54, 1983.

Hartmann, D. L., A PV View of Zonal Flow Vacillation, *J. Atmos. Sci.*, *52*, 2561-2576, 1995.

Hayashi, Y., A generalized method of resolving disturbances into progressive and retrogressive waves by space Fourier and time cross spectral analyses, *J. Meteorol. Soc. Japan*, *49*, 125-128, 1971.

Hoskins, B. J., M. E. McIntyre, and A. W. Robertson, On the use and significance of isentropic potential vorticity maps, *Q. J. R. Meteorol. Soc.*, *111*, 877-946, 1985.

Mote, P. W., J. R. Holton, and J. M. Wallace, Variability in total ozone associated with baroclinic waves, *J. Atmos. Sci.*, *48*, 1900-1903, 1991.

Newell, R. E., Y. Zhu, E. V. Browell, S. Ismail, W. G. Read, J. W. Waters, K. K. Kelly and S. C. Liu, Upper tropospheric water vapor and cirrus: Comparison of DC-8 observations, UARS microwave limb sounder measurements and meteorological analyses, *J. Geophys. Res.*, *101*, 1931-1941, 1995.

Randel, W. J. and J. L. Stanford, An observational study of medium-scale wave dynamics in the Southern Hemisphere summer. Part I: Wave structure and energetics, *J. Atmos. Sci.*, *42*, 1172-1188, 1985.

Read, W. G., J. W. Waters, D. A. Flower, L. Froidevaux, R. F. Jarnot, D. L. Hartmann, R. S. Harwood, and R. B. Rood, Upper-tropospheric water vapor from UARS MLS, *Bull. Amer. Met. Soc.*, *76*, 2381-2389, 1995.

Rodgers, E. B., V. V. Salomonson, and H. L. Kyle, Upper tropospheric dynamics as reflected in Nimbus 4 THIR 6.7-μm data, *J. Geophys. Res.*, *81*, 5749-5758, 1976.

Salby, M. L., A ubiquitous wavenumber-5 anomaly in the Southern Hemisphere during FGGE, *Mon. Wea. Rev.*, *110*, 1712-1720, 1982.

Schoeberl, M. R., and A. J. Krueger, Medium scale disturbances in total ozone during Southern Hemisphere summer, *Bull. Amer. Meteor. Soc.*, *64*, 1358-1365, 1983.

Simmons, A. J. and B. J. Hoskins, The life cycles of some nonlinear baroclinic waves, *J. Atmos. Sci.*, *35*, 414-423, 1978.

Thorncroft, C. D., B. J. Hoskins and M. E. McIntyre, Two paradigms of baroclinic-wave life-cycle behaviour, *Q. J. R. Meteorol. Soc.*, *119*, 17-55, 1993.

Trenberth, K. E., Global Analyses from ECMWF and Atlas of 1000 to 10mb Circulation Statistics, *NCAR Tech. Note NCAR/TN-373+STR*, 191 pp., 1992.

W. J. Randel and E. M. Stone, National Center for Atmospheric Research, Boulder, CO 80307. (e-mail: emstone@acd.ucar.edu)

J. L. Stanford, Department of Physics and Astronomy, Iowa State University, Ames, IA 50011.

W. G. Read, and J. W. Waters, Jet Propulsion Laboratory, California Institute of Technology, Pasadena, CA 91109.

(Received July 16, 1996; accepted August 12, 1996)